The Intracellular Loop of the Na^{+}/Ca^{2+} Exchanger Contains an “Awareness Ribbon” Shaped Two-helix Bundle Domain

Jiaqi Yuan[1], *Chunhua Yuan*[2], *Mouzhe Xie*[1], *Lei Yu*[1], *Lei Bruschweiler-Li*[2],

and Rafael Brüschweiler[*,1,2,3]

[1]Department of Chemistry and Biochemistry, The Ohio State University, Columbus, Ohio 43210, USA

[2]Campus Chemical Instrument Center, The Ohio State University, Columbus, Ohio 43210, USA

[3]Department of Biological Chemistry and Pharmacology, The Ohio State University, Columbus, Ohio 43210, USA

ABSTRACT

The Na^+/Ca^{2+} exchanger (NCX) is a ubiquitous single-chain membrane protein that plays a major role in regulating the intracellular Ca^{2+} homeostasis by the counter transport of Na^+ and Ca^{2+} across the cell membrane. Other than its prokaryotic counterpart, which contains only the transmembrane domain and is self-sufficient as an active ion transporter, the eukaryotic NCX protein possesses in addition a large intracellular loop that senses intracellular calcium signals and controls the activation of ion transport across the membrane. This provides a necessary layer of regulation for the more complex function of eukaryotic cells. The Ca^{2+} sensor in the intracellular loop is known as the Ca^{2+}-binding domain (CBD12). However, how the signaling of the allosteric intracellular Ca^{2+} binding propagates and results in transmembrane ion transportation still lacks a detailed explanation. Further structural and dynamics characterization of the intracellular loop flanking both sides of CBD12 is therefore imperative. Here, we report the identification and characterization of another structured domain that is N-terminal to CBD12 in the intracellular loop using solution nuclear magnetic resonance (NMR) spectroscopy. The atomistic structure of this domain reveals that two tandem long α-helices, connected by a short linker, form a stable cross-over two-helix bundle (THB), resembling an "awareness ribbon". Considering the highly conserved amino acid sequence of the THB domain, the detailed structural and dynamics properties of the THB domain will be common among NCXs from different species and will contribute toward the understanding of the regulatory mechanism of eukaryotic Na^+/Ca^{2+} exchangers.

INTRODUCTION

The Na^+/Ca^{2+} exchanger (NCX) plays a key role in maintaining cellular Ca^{2+} homeostasis of excitable cells, such as neuron and muscle cells, as well as non-excitable cells.[1-4] By making use of the Na^+ electrochemical gradient across the membrane, the NCX protein transports Ca^{2+} to the opposite side of the membrane in exchange with Na^+ with a 1:3 Ca^{2+}/Na^+ stoichiometry.[5] NCX has high turnover rate, which enables cells the rapid efflux of large amounts of Ca^{2+} required for their physiological function. The NCX protein dysfunction is related to the alteration of calcium homeostasis in serious diseases, including stroke and heart failure.[6,7]

There are three genes encoding NCX proteins, termed *ncx1*, *ncx2*, and *ncx3*. There are also alternative splice variants of *NCX1* and *NCX3*. NCX isoforms express in tissue specific and cell specific manner.[6,8] Alternative splicing isoforms of NCX1 are encoded by the mutually exclusive exon A or B and Cassette exons C-F. Previous biochemical based topology studies of eukaryotic NCX protein suggested that NCX consists of a transmembrane domain (TM1-TM10) that is responsible for ion recognition and exchange, and a large intracellular loop (f-loop), which connects TM5 and TM6 and accounts for almost half the size of NCX (Figure 1).[9] The f-loop is implicated in the secondary Ca^{2+} regulation of the ion transport of NCX.[10] Although the structure of the eukaryotic NCX is not available, the crystal structure of its prokaryotic ortholog from *Methanococcus jannaschii*, termed NCX_Mj, has been determined.[11] The structure shows ten transmembrane α-helices (TM1 – TM10) arranged in two symmetric halves, which is considered to be a realistic model of the structure of the eukaryotic NCX protein transmembrane domain.[12,13] Recent studies of NCX_Mj crystal structures of apo and its various ion-bound forms indicate that the outward-to-inward transition of the transmembrane domain during ion translocation is controlled by the ion-occupancy of four ion-binding sites located in the center of the transmembrane domain.[14,15] Since NCX_Mj however does not contain the f-loop, the regulatory role of the eukaryotic intracellular loop cannot be explained using this model system.

The f-loop contains a Ca^{2+}-binding tandem domain CBD12 (CBD1 and CBD2) located at the center, and largely disordered regions flanking the CBD12 domain, termed Cyto1 and Cyto2 for cytoplasmic segment 1 (at the N-terminus of the loop) and cytoplasmic segment 2 (at the C-terminus of the loop) (Figure 1). CBD1 and CBD2 each adopt a β-sandwich structure similar to the C2 domain, and their Ca^{2+} binding sites are located at the tip of each domain.[16-18] Our previous study of the canine NCX1 AD isoform (where exon A and exon D are expressed) of CBD12 domain showed for the first time that the primary structural effect of Ca^{2+} binding is the rigidification of CBD12 in an elongated conformation, which is likely the structural trigger for NCX ion transportation.[19] This work was subsequently confirmed by hydrogen/deuterium-exchange mass spectrometry.[20-22]

How the conformational and dynamics changes of CBD12 in the center of the intracellular loop are communicated to the transmembrane domain of NCX over a distance of several tens of Å to regulate ion transportation is intriguing.[23,24] We recently proposed that this allosteric effect is largely entropy-driven as captured by a Gaussian chain model for the intrinsically disordered parts of the intracellular loop.[25] Upon intracellular Ca^{2+} binding, the rigidified, elongated CBD12 domain restricts the overall mobility of the entire intracellular loop and thereby exerts a force on the TM domain that triggers a conformational change enabling ion transport. Since the magnitude of the force critically depends on the geometric dimension of the intracellular loop, detailed information about the structure of the entire loop region at atomic resolution is important as it has direct consequences for the better understanding of the activation mechanism of NCX.

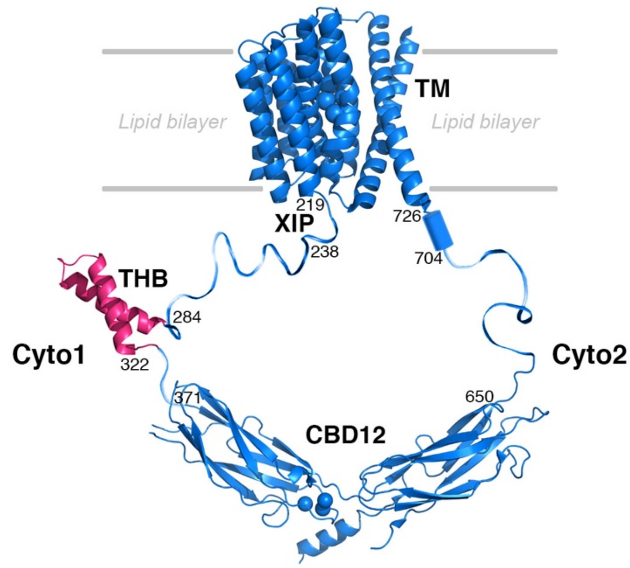

Figure 1. Schematic representative of eukaryotic NCX1 structure. Updated model of NCX1 of canine AD splice variant consists of a transmembrane domain TM (residue 1-218 and 727-903, represented by PDB 3V5U of NCX_Mj) and an intracellular f-loop (219-726) where the numbering is based on the AD isoform of mature full length protein. Several domains and regions are part of the intracellular loop: exchanger inhibitory peptide XIP (residues 219-238), two-helix bundle domain THB (PDB 6BV7, residue 284-322), Ca^{2+} binding domain CBD12 (PDB 3US9, CBD1 residues 371-500 and CBD2 501-650), cytoplasmic segment 1 Cyto1 (residues 219-370), cytoplasmic segment 2 Cyto2 (residues 651-726).

Our recent NMR study of a major portion of Cyto2 (657-702) demonstrated this region to be intrinsically disordered (see also Figure S1).[25] A short α-helix was predicted at the C-terminus of Cyto2 (between 704-726) (Figure 1).[26,27] These results suggest that Cyto2 is largely disordered. Within Cyto1, it has been shown that the highly positively charged 20-residue exchanger inhibitory peptide (XIP) located at the N-terminus of the f-loop is likely to be random coil.[28,29] This leaves the rest of Cyto1, which contains about 130 residues, the only region of the f-loop of

NCX that has not been experimentally characterized. Despite very low sequence similarity, it was previously proposed that this region forms an α-catenin-like domain (CLD) together with the distant Cyto2 region and a model for the function of the f-loop was put forward.[30] Experimental characterization of the region of Cyto1 encompassing the 130 residues is expected to shed more light on the f-loop regulatory role.

Here, we report the only structured region within the 130 residues and determine its high-resolution 3D NMR structure. This structure is a two-helix bundle (THB) formed by 39 residues, flanked by disordered residues. Our study completes the structural characterization of the structured domains of NCX and permits the development of mechanistic models of NCX activation.

MATERIALS AND METHODS

Plasmid Construction

THB domain encoding canine NCX1 AD splice variant 274-327 was amplified from canine cerebellum cDNA where primers 5'-TACTTCCAATCCAATGCAGTTCTGGAGGTTGATGAGAGGGACCAAGATGATGAAGAG-3' and 5'-TTATCCACTTCCAATGTCATGCTCGGCTTTTCTGCTGCTGACTTAGGACTTGGTAGTTAG-3' were used. PCR product was cloned into vector pTBSG1[31] containing hexa-histidine tag and TEV cleavage site at N-terminus, the resulting plasmid pTBSG1-NCX274-327 was transformed into *Escherichia coli* (*E.coli*) DH5α using ligation independent cloning.[32] After sequencing at Genewiz, confirmed plasmids were transformed into *E.coli* BL21(DE3) competent cells for protein overexpression. Genes encoding canine NCX1 AD isoform 285-366 (pTBSG1-NCX285-366) was constructed in the same way, using primers 5'-TACTTCCAATCCAATGCAGAAGAGGCGAGGCGAG

AAATGGCTAGGA-3’ and 5’-TTATCCACTTCCAATGTCAAGCCACTTCAGTGTTGACCTCATGC ATGCT-3’.

Protein Expression and Purification

E.coli BL21(DE3) cells containing pTBSG1-NCX274-327 were inoculated in 40 mL LB for overnight growth at 37 ˚C. The cell culture was harvested by centrifuging at 5000 rpm for 20 min and the cells were transferred to 1 L M9 minimal medium using 1 g/L ^{15}N-labeled NH_4Cl and 4 g/L ^{13}C-labeled glucose as the sole nitrogen and carbon sources, respectively, to obtain uniformly ^{15}N and ^{13}C labeled protein. When the culture OD_{600} reached 0.7, IPTG was added into the inoculum at final concentration of 0.5 mM to induce protein expression for 4 hrs at 37 °C. After harvesting, the cells were lysed with emusiflex C5 homogenizer (Avestin). Supernatant was loaded to a Ni-NTA column (Qiagen). Buffers containing 50 mM sodium phosphate pH 7.0, 500 mM NaCl, with an imidazole gradient were used to wash away non-specific bounding, and a final concentration of 250 mM imidazole was used for elution. The His-tag of NCX274-327 was cleaved overnight with TEV protease, and the protein was further purified using a Ni-NTA column. The protein sample was loaded into an Amicon Ultra centrifugal device (Millipore) with MWCO of 3 kD to perform protein buffer exchange and concentration. The final protein concentration was 300 μM, in NMR buffer containing 20 mM sodium phosphate pH 7.0, and 100 mM NaCl. Uniformly ^{15}N, ^{13}C-labeled protein was either directly prepared in the NMR buffer supplemented with 10% D_2O, or lyophilized and reconstituted in 100% D_2O before NMR measurement (detailed sample conditions for each NMR experiment are part of the PDB entry). Construct pTBSG1-NCX285-366 was overexpressed and purified following the same protocol, except the cells were induced for 6 hrs at 16 °C.

NMR Spectroscopy

All NMR spectra were acquired at 298 K on Bruker AVANCE III spectrometers, either at 700 MHz equipped with a TXO cryoprobe or at 850 MHz with a TCI cryoprobe. 2D ^{15}N-^{1}H HSQC was collected as a reference. The THB domain backbone assignments were achieved by recording BEST-type triple resonance experiments HNCA, HNCOCA, HNCO, HNCACO, HNCACB and HNCOCACB.[33,34] Side-chain assignments were obtained from HCCH-TOCSY, (H)CCH-TOCSY, H(CCO)NH-TOCSY and (H)CC(CO)NH-TOCSY experiments. High-resolution CT ^{13}C-^{1}H HSQC was collected to obtain accurate side-chain assignments. Chemical shifts and NOEs of aromatic rings were analyzed from 2D aromatic TROSY-HSQC and 2D ^{1}H homonuclear NMR experiments in D_2O. 3D HNHB and 2D DQF-COSY were recorded to assist χ_1 dihedral angle identification together with relative NOE intensities.[35,36] 2D CT ^{13}C-^{1}H HSQC was acquired using 10% ^{13}C-labeled protein sample for stereospecific assignments of the methyl groups of Val and Leu residues.[37] A series of isotope-edited 3D NOESY spectra were collected including 3D ^{15}N-edited NOESY, 3D ^{15}N-edited CNH-NOESY,[38] 3D ^{13}C-edited NOESY and 3D ^{13}C-edited CCH-NOESY. Mixing time in all NOESY experiments was 180 ms. Backbone ^{15}N R_1 and R_2 relaxation rates were obtained from conventional R_1 and $R_{1\rho}$ spin relaxation experiments in a pseudo-3D fashion, where the intensities of ^{15}N-^{1}H HSQC-style cross-peaks were recorded as a function of six relaxation delay intervals (R_1 = {0.04, 0.20, 0.50, 0.80×2, 1.20 s}, $R_{1\rho}$ = {2, 24, 48, 72×2, 96 ms}). The R_2 rates were then determined from the R_1 and $R_{1\rho}$ rates as well as the resonance offsets for each cross-peak. {^{1}H}-^{15}N steady-state nuclear Overhauser effect was measured using standard ^{15}N relaxation methods.[39,40] Triple resonance experiments for backbone assignments and the {^{1}H}-^{15}N heteronuclear NOEs of construct 285-366 were obtained under the same conditions as for THB domain. All NMR spectra were processed with NMRPipe and visualized using NMRView and Sparky.[41-43]

Structure Calculation

Backbone φ, ψ dihedral angle constraints were obtained from the backbone chemical shifts using TALOS+.[44] Side-chain χ_1 dihedral angle constraints were deduced from $^{3}J_{H^\alpha,H^\beta}$ and $^{3}J_{N,H^\beta}$ coupling constants and NOE measurements. The NOE cross-peaks were categorized into strong, medium, weak, and very weak NOEs, corresponding to upper distance restraints of 2.7, 3.7, 5.0, and 6.0 Å, respectively.

The above constraints together with the hydrogen-bond constraints identified in the secondary structure elements were used as input for CNS 1.3 for 3D structure calculations with a simulated annealing protocol.[45] Further dihedral angle validation was done by PSVS.[46] As observed previously, backbone angles in disallowed regions are produced by the CNS software for residues that have a very limited number of constraints.[47] 20 out of 100 structures were selected based on least NOE violations, RMSD, and the lowest energy. RMSD was calculated using MOLMOL.[48] Structure and molecular graphics were generated using PyMOL and MOLMOL. Electrostatic potential was calculated and visualized using PDB2PQR and APBS.[49,50] The backbone and side-chain assignments were deposited in BMRB under the accession number 30379. THB domain protein structure was deposited in the PDB (ID 6BV7).

Molecular Dynamics Simulation

The simulation was performed using GROMACS 5.0 package.[51] AMBER99SBnmr1-ILDN was used as the force field,[52] and water molecules were explicitly included using TIP4P-D water model.[53] The integration step was set to 2 fs with all bond containing hydrogen atoms restrained by the SETTLE algorithm. Na^+ ions were added to neutralize the total charge of the system. A cutoff of 10 Å was used for all van der Waals and electrostatic interactions. Particle-Mesh Ewald summation with a grid spacing of 1.2 Å was used to calculate long-range electrostatic interactions. A cubic simulation box that extends 8 Å from the protein surface was used, and periodic boundary conditions were applied in all three dimensions. After 50,000 steps of steepest descent energy minimization, the system was simulated for 100 ps at a constant temperature of 298 K and constant volume with all protein heavy atoms fixed. Next, pressure was coupled at 1 atm and the system was simulated for another 100 ps. The final production run was performed in the NPT ensemble at 298 K and 1 atm. The RMSD of the Cα (residues 284-322) from each snapshot was calculated compared with the initial structure. The angle between the two α-helices was calculated based on the helical directions determined by principle component analysis using backbone atomic coordinates, as specified in Supporting Information.

RESULTS

Cyto1 of intracellular loop of eukaryotic NCX has a structured domain

Sequence-based secondary structure prediction of residues 239-370 (between XIP and CBD12) of the canine NCX1 AD isoform was performed (residue numbering in this study is based on the AD isoform of mature full length protein) (Figure 1). Both Psipred and I-TASSER[54,55] predicted an α-helix-rich region (4-5 helices spanning residues 279-366) flanked by disordered residues (Figure S2). We then overexpressed ^{15}N, ^{13}C-isotopically labeled region 285-366 and obtained residue-specific assignments of N_H, H_N, $C\alpha$, $H\alpha$, $C\beta$, and CO nuclei. Based on these chemical shifts, secondary structure propensity (SSP) analysis[56] was performed (Figure 2). In general, the larger the value of the SSP, the higher the probability that a residue belongs to an α-helix. Our SSP analysis identified two potential long helices encompassing residues 285-301 and 307-323 with absolute SSP values > 0.5. These two α-helices approximately coincide with the first two predicted helices starting from the N-terminus. The absolute SSP values of residues 327-366 near the C-terminus are below 0.3, indicating that these residues predominantly adopt a random coil with minimal local secondary structure, rather than 2 or 3 helices suggested by the *in silico* predictions. In order to further corroborate the SSP results, $\{^1H\}$-^{15}N steady-state nuclear Overhauser effect (hetNOE) parameters were measured. The hetNOE of residues 285-301 and 307-323 are above 0.6, which is typical for structured regions, whereas hetNOE values of residues 325-366 are either close to zero or even negative, indicative of large-scale dynamics on the ps-ns timescale characteristic of random coil. Hence, both SSP and hetNOE parameters pinpoint the locations of the two helices and the disordered regions.

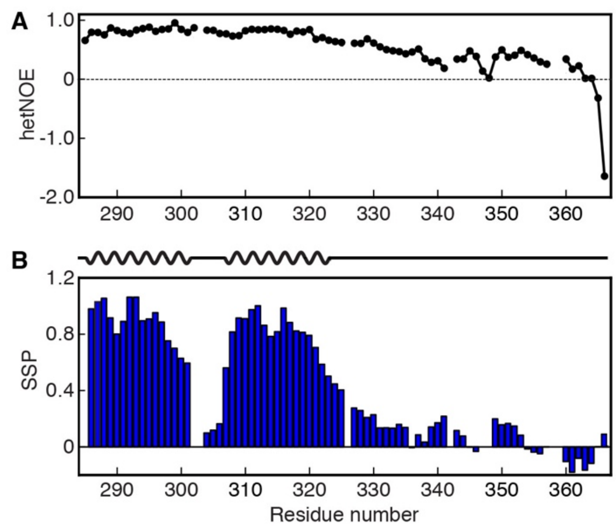

Figure 2. Secondary structure analysis of canine NCX1 residues 285-366. A. {^{1}H}-^{15}N hetNOE of residues 285-366. Missing data points belong to residues whose chemical shifts could not be unambiguously assigned. B. SSP of residues 285-366. Regions 285-301 and 307-323 have high helicity (SSP > 0.5).

THB forms a compact helical domain

Because the N-terminal residue 285 appears to initiate the first helix, it is possible that in the full-length native sequence the helix may start with a residue N-terminal to residue 285. In order to accurately characterize the entire helical region, we adjusted the length of the construct to include residues 274-327. The 2D NMR ^{15}N-^{1}H HSQC spectrum of residues 274-327 (Figure 3) retains virtually all of the well-dispersed cross-peaks in the previous construct, indicating that the peptide adopts a folded structure. A standard suite of triple resonance NMR experiments performed on a uniformly ^{15}N, ^{13}C-labeled sample was carried out, and 97.8% of the chemical shifts were assigned, including 100% of the backbone N_H, H_N, Cα, Hα, and CO atoms, and 96.6% of the assignable spin one half side-chain atoms.[57]

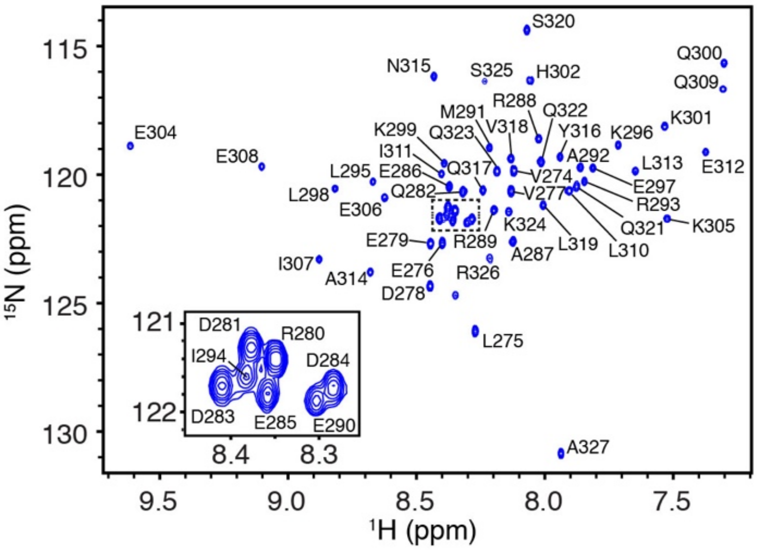

Figure 3. ^{15}N-^{1}H HSQC spectrum of NCX1 THB domain with residue assignments indicated. For clarity, only the region of backbone amides is shown in the figure. The cross-peak without label (above cross-peak L275) corresponds to a remaining Ala residue after TEV cleavage.

In order to obtain distance constraints between proton pairs for 3D structure determination, a series of 3D ^{15}N-edited and ^{13}C-edited NOESY data were collected. Many short-range NOE connectivities characteristic of α-helices, such as $d_{\alpha\beta(i,i+3)}$, were observed and summarized in Figure 4, which confirmed the existence of two long α-helices. Next, a high-resolution 3D structure of the THB domain was calculated based on the experimentally derived distance and dihedral angle constraints (Table 1). An ensemble of 20 structures was selected from 100 computed structures on the basis of the least constraint violations and lowest energy. It shows that the structured region starts from residue D284, and the two long α-helices contain residues 284-301 and 307-322 respectively, as predicted in the SSP analysis. Hence, the structured THB domain has been identified to consist of 39 residues covering residues 284 to 322.

Figure 4. Summary of NMR-derived NOE connectivities of NCX1 THB domain. The bars correspond to experimentally observed short-range NOEs defined on the left-hand side. Some NOEs in the two long helical stretches (residues 284-301 and 307-322) are missing due to peak overlap.

For residues in the THB domain, the ensemble has an average backbone root-mean-square deviation (RMSD) of 0.41 ± 0.10 Å and an average heavy atom RMSD of 1.00 ± 0.11 Å. The Ramachandran plots of the backbone dihedral angle distributions indicate a good overall protein structure quality, as virtually all residues in the structured part (residues 284-322) fall into the most favored regions and none in the disallowed regions. We also calculated structures without H-bond constraints (structure refinement statistics are summarized in Table S1), which are very similar to the ones reported in Table 1.

Table 1. NMR structure refinement statistics of NCX1 THB domain.

Distance restraints	
Total NOE	687
Intraresidue	271
Interresidue	
Sequential (|i-j|=1)	179
Medium range (1<|i-j|<5)	197
Long range ((|i-j|≥5)	40
Hydrogen bonds	28
Total dihedral angle restraints	
φ	34
ψ	34
χ	7[a]
Residual restraint violations	
Bond lengths, Å	0.0055 ± 0.0001
Bond angles, °	0.44 ± 0.01
Impropers, °	0.171 ± 0.005
Distance violations (>0.3 Å)	0
Dihedral angle violations (>5°)	0
Deviation from idealized geometry	
Number of close contacts	0
Bond angles, °	0.5°
Bond lengths, Å	0.008
Average pairwise rmsd[b]	
All heavy atoms, Å	1.00 ± 0.11
Backbone atoms, Å	0.41 ± 0.10
Ramachandran statistics from Procheck	
Most favored	95.2%
Additionally allowed	3.6%
Generously allowed	0.0%
Disallowed	1.1%
Procheck Z-scores	
phi-psi	-1.1
All	-1.4
MolProbity Clashscore	0.3

[a]Residues are I294, H302, I311, L313, N315, V318 and S320. Stereospecific assignments for $H_{\beta2}$ and $H_{\beta3}$ protons were obtained for H302, L313, N315, and S320 residues.
[b]Pairwise rmsd was calculated for residues 284-322.

The 3D THB domain structure, depicted in Figure 5A, shows an "awareness ribbon" like conformation, composed of two long α-helices connected by a short 5-residue linker that assumes a turn. The angle between the two antiparallel helices is 132.9° ± 2.4°, which is defined by inter-helical interactions, hydrophobic effects, and long-range NOEs. Long-range NOEs are observed for hydrophobic residues M291, I294, L295, L298, L310, I311, A314, and V318 (Figure 5C), involving both backbone and side-chain protons. Specifically, long-range NOEs I294-V318, L298-A314, and H302-L310 reflect close contacts between the helices (Figure S3B) and the four leucine residues L295, L298, L310, and L313 form a hydrophobic stack (Figure S3C). The helical wheel diagram (Figure S3A) reflects an amphipathic nature of both helices. This is consistent with the electrostatic potential of the THB domain (Figure 5B), which demonstrates that the hydrophobic residues occupy only a small surface area whereas the hydrophilic residues tend to be oriented toward the solvent. These results suggest that the two helices are stabilized largely by hydrophobic contacts. In terms of other forces, electric dipole-dipole interactions between the two anti-parallel α-helices are likely also contributing to stability, in addition to the helix-capping[58] effect as evidenced by an NOE observed between E306 H_N and Q309 side-chain amide protons. The proline residue of the short linker 302-306 with sequence HPEKE is in a trans configuration, as evidenced by the strong sequential NOEs between H302 H_α and P303 $H_{\delta 1}/H_{\delta 2}$[59].

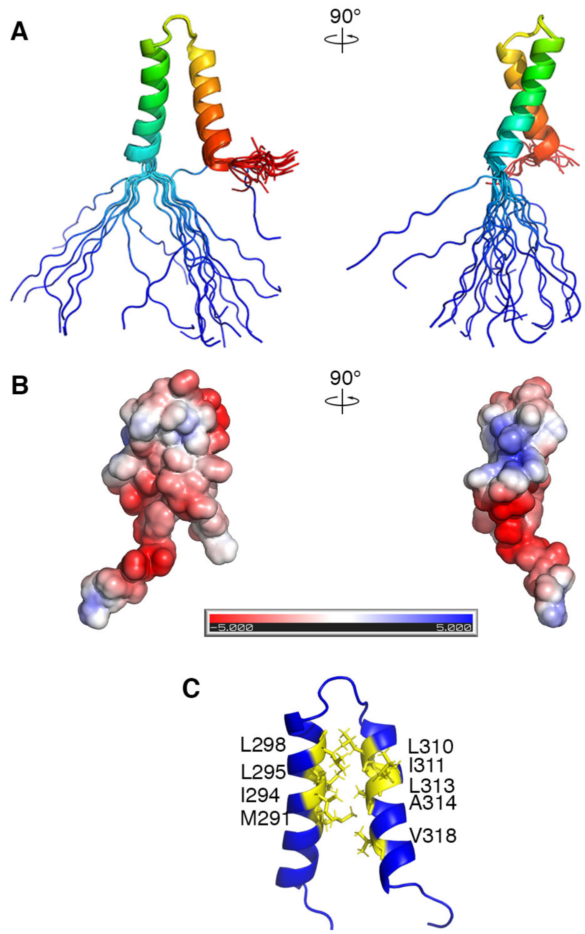

Figure 5. 3D structure of THB domain. A. Ribbon diagram of solution NMR structure ensemble of THB domain of 20 structures with least restraint violations and lowest energy. Structures are spatially aligned with respect to the ordered region 284-322. B. Electrostatic potential from –5 kT/e (red) to 5 kT/e (blue) on the surface of a low energy structure of THB domain calculated using APBS software.[45] C. Depiction of the packing of hydrophobic core residues (yellow) of THB domain.

To assess the stability of the NMR structure of the THB domain, a molecular dynamics (MD) simulation was performed for a total length of 500 ns with the Amber99SBnmr1-ILDN force field in TIP4P-D explicit water[52,53] starting from the lowest energy NMR structure. The backbone RMSD of individual snapshots relative to the NMR structure shows a stable behavior fluctuating around 5 Å with an average inter-helical angle of 124.2º (Figure S4), which is close to the one of the NMR structures. These results confirm the stability of the NMR structure of the THB domain.

THB dynamics on ns-ps timescale

NMR ^{15}N spin relaxation experiments provide atomic-detail information about ns-ps timescale dynamics of backbone ^{15}N-^{1}H bond vectors. In order to characterize the internal mobility of the THB domain, backbone ^{15}N longitudinal relaxation rates (R_1), transverse relaxation rates (R_2) and {^{1}H}-^{15}N hetNOE data were measured and the results are shown in Figure 6. As expected, residues 284-301 and 307-322 corresponding to the α-helices show overall higher R_1, R_2, and hetNOE values compared to the random coil regions at the two termini. The average experimental tumbling correlation time τ_c extracted from backbone ^{15}N relaxation data of the N-H vectors of the two helices is 4.75 ns, which is in general agreement with τ_c = 4.19 ns predicted by HYDRONMR[60] when only the helical regions were used as input, i.e. after the flexible tails were removed. The average tumbling correlation time (rank 2) of the N-H vectors of the helices was also directly calculated from the MD simulation of the THB monomer yielding 4.80 ns. This is consistent with a recent MD study, which found that the tumbling correlation times of proteins are quite well reproduced by the TIP4P-D water model used here.[61] Together, these results suggest that THB is monomeric and unlikely to induce dimerization of NCX[62] under *in vitro* condition, which is also consistent with the absence of intermolecular NOEs for THB. Interestingly, the linker residues 302-306 have an average hetNOE above 0.8, which is similar to the hetNOEs displayed by the helices. This indicates that the linker is relatively rigid on the ps-ns timescale, which is also confirmed by its R_1 and R_2 values.

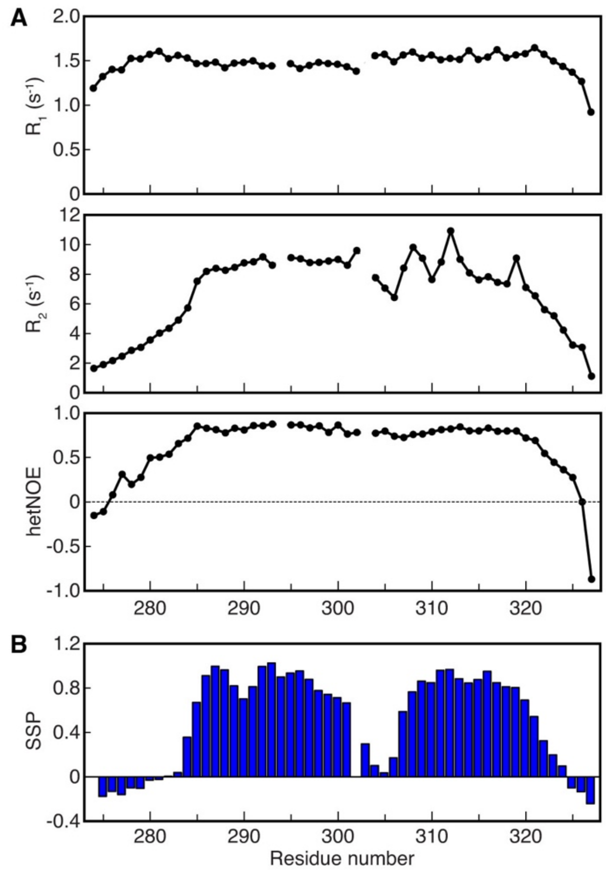

Figure 6. NMR ^{15}N spin relaxation data and SSP of NCX1 THB domain. A. ^{15}N R_1, R_2 and $\{^1H\}$-^{15}N hetNOE data of THB domain (missing data points belong to I294 and P303). B. Secondary structure propensity (SSP) of NCX1 THB domain.

DISCUSSION AND CONCLUSION

The newly identified THB domain in the NCX f-loop is well-defined and consists of two tightly packed α-helices connected by a short linker, resembling an "awareness ribbon", and it is flanked by intrinsically disordered regions. This work completes the structural characterization of the major building blocks of the overall NCX protein architecture. Considering that secondary Ca^{2+} regulation is mediated via the intracellular loop, knowledge of the existence and exact shape of the THB domain is essential for the detailed understanding of the ion transport mechanism of NCX.

Recently, we proposed a Gaussian chain model for the disordered portions of the intracellular loop to rationalize regulation of the ion transport in the transmembrane domain.[25] The Gaussian chain model, which is commonly used for the interpretation of functional aspects of intrinsically disordered proteins,[63] can explain a wealth of experimental data of the NCX system. When Ca^{2+} ions bind to CBD12, which is a predominantly enthalpy-driven process and results in the rigidification of CBD12 in an elongated conformation, lateral forces are generated that act on the transmembrane domain inducing a conformational change that enables ion transport. Because the number of conformational microstates of the intracellular loop is lowered upon Ca^{2+} binding, these forces are largely entropy-driven, analogous to the restoring force of an extended rubber band. The lateral force can be expressed as:

$$f = \frac{2k_B T}{L_{CBD12}} - \frac{3k_B T L_{CBD12}}{NL^2} \tag{1}$$

where L_{CBD12} is the end-to-end distance of CBD12, L is the average length of an amino acid, and N is the number of disordered residues. Since in our previous work, the structure of the helical region characterized here was still missing, the THB domain structure provides essential new atomic-detail information to refine the molecular force mechanism that enables ion transport. Because the region that encompasses the THB domain is folded, rather than intrinsically disordered, its net effect is a shortening of the intrinsically disordered portion of the intracellular loop, which is reflected in a reduction of N in Eq. (1). As a consequence, the lateral force increases since it is inversely proportional to the length of the disordered portion of the chain (Eq. (1)), which is likely to enable larger structural changes in the transmembrane domain necessary for ion transport. ^{15}N R_1 and R_2 NMR relaxation data at pH 5.5 and pH 8.0 showed similar values compared to pH 7.0 (data not shown), indicating that the fold of the THB domain is stable within a wide pH range and, itself, may not be subject to significant structural perturbation during allosteric activation of NCX. If, however, *in vivo* conditions exist that cause a break-up of the helix-helix interactions of THB, it would significantly increase the effective size of the intracellular loop and, hence, diminish or even abolish its ability to modulate the structure of the transmembrane helices for ion transport.

It was previously proposed based on sequence analysis that Cyto1 and Cyto2 form a well-defined catenin-like domain (CLD), whereby residues 273-285, 288-301, 311-316, 323-352, and 357-368 in Cyto1 region form 5 α-helices [30]. Our present experimental work unambiguously shows that there are only 2 α-helices in this region formed by residues 284-301 and 307-322 in the THB domain whereas the rest are disordered. In addition, our recent NMR characterization of Cyto2 demonstrated its intrinsic disorder (Figure S1).[25] Therefore, it is unlikely that Cyto1 or Cyto2 form a CLD. To investigate whether there is a folding-upon-binding event, we recorded ^{15}N-^{1}H HSQC spectra of ^{15}N-labeled THB domain that included the disordered tails (residues 274-327) in the presence and absence of non-labeled Cyto2 (residues 657-702). No chemical shift perturbations however were observed (Figure S5), suggesting that Cyto2 does not alter the structure of Cyto1. The previously proposed model of a CLD domain in the NCX f-loop requires revision as it is at variance with the experimental data reported here.

Given the ubiquitous presence of NCX proteins among mammalian species, we performed sequence alignment of NCX1 protein sequences from multiple species (Figure 7). The results revealed a remarkably high sequence identity of the 274-366 region among all the species: all residues in the THB domain are fully conserved except for residue 304, which is either Asp or Glu. Residues 328-362, which form the region immediately C-terminal to the THB domain, are also highly conserved among these species. Based on the extraordinarily high level of sequence conservation, the structure determined here for canine NCX1 should be directly transferable to other species that share an identical or highly similar sequence for this part of the intracellular loop, such as human NCX1. Moreover, secondary structure predictions using I-TASSER identified two helical structures connected by a short linker in human NCX2 and NCX3 in the region corresponding to NCX1 THB domain as demonstrated in the sequence alignment (Figure S6). Helical wheel analysis shows that these two helices are also amphipathic, as for the NCX1 THB helices. Thus, they most likely adopt the same “awareness ribbon” like structures. Since *Drosophila* CALX is regulated in the opposite manner to NCX (i.e. high Ca^{2+} concentration disables ion exchange),[64] it is perhaps not too surprising that it shares low similarity with the NCX1 sequences (Figure S7) and the loop structure and/or dynamics of CALX may differ from canine NCX1 determined in this work. Information about the exact location and 3D structure of the THB domain presented here enables new hypotheses about the role of this domain by investigating how mutations of key residues that stabilize THB intradomain interactions, or the knockout of the entire THB domain, affect signaling between the intracellular loop and the transmembrane domain. Techniques, such as patch clamp, could be applied to full-length NCX with altered sequences to help better understand the relationship between the atomic properties of this two-helix bundle and the physiological function of NCX.

```
                   251                 261                 271                 281                 291
Canis lupus        K T E I E M D G K V V N S H V D N F L D G A L V L E V D E R D Q D D E E A R R E M A R I L K E L K Q
Homo sapiens       K T E I E M D G K V V N S H V E N F L D G A L V L E V D E R D Q D D E E A R R E M A R I L K E L K Q
Macaca mulatta     K T E I E M D G K V V N S H V E N F L D G A L V L E V D E R D Q D D E E A R R E M A R I L K E L K Q
Felis catus        K T E I E M D G K V V N S H V D N F L D G A L V L E V D E R D Q D D E E A R R E M A R I L K E L K Q
Ratus norveficus   K T E I E M D G K V V N S H V D N F L D G A L V L E V D E R D Q D D E E A R R E M A R I L K E L K Q
Mus musculus       K T E I E M D G K V V N S H V D N F L D G A L V L E V D E R D Q D D E E A R R E M A R I L K E L K Q
                   * * * * * * * * * * * * * * * : * * * * * * * * * * * * * * * * * * * * * * * * * * * * * * * * * *

                   301                 311                 321                 331                 341
Canis lupus        K H P E K E I E Q L I E L A N Y Q V L S Q Q Q K S R A F Y R I Q A T R L M T G A G N I L K R H A A D
Homo sapiens       K H P D K E I E Q L I E L A N Y Q V L S Q Q Q K S R A F Y R I Q A T R L M T G A G N I L K R H A A D
Macaca mulatta     K H P E K E I E Q L I E L A N Y Q V L S Q Q Q K S R A F Y R I Q A T R L M T G A G N I L K R H A A D
Felis catus        K H P E K E I E Q L I E L A N Y Q V L S Q Q Q K S R A F Y R I Q A T R L M T G A G N I L K R H A A D
Ratus norveficus   K H P D K E I E Q L I E L A N Y Q V L S Q Q Q K S R A F Y R I Q A T R L M T G A G N I L K R H A A D
Mus musculus       K H P E K E I E Q L I E L A N Y Q V L S Q Q Q K S R A F Y R I Q A T R L M T G A G N I L K R H A A D
                   * * * : * * * * * * * * * * * * * * * * * * * * * * * * * * * * * * * * * * * * * * * * * * * * * *

                   351                 361                 371                 381                 391
Canis lupus        Q A R K A V S M H E V N T E V A E N D P V S K I F F E Q G T Y Q C L E N C G T V A L T I I R R G G D
Homo sapiens       Q A R K A V S M H E V N T E V T E N D P V S K I F F E Q G T Y Q C L E N C G T V A L T I I R R G G D
Macaca mulatta     Q A R K A V S M H E V N T E V T E N D P V S K I F F E Q G T Y Q C L E N C G T V A L T I I R R G G D
Felis catus        Q A R K A V S M H E V N T E V A E N D P V S K I F F E Q G T Y Q C L E N C G T V A L T I L R R G G D
Ratus norveficus   Q A R K A V S M H E V N M D V V E N D P V S K V F F E Q G T Y Q C L E N C G T V A L T I I R R G G D
Mus musculus       Q A R K A V S M H E V N M E M A E N D P V S K I F F E Q G T Y Q C L E N C G T V A L T I M R R G G D
                   * * * * * * * * * * * *   : : . * * * * * * * : * * * * * * * * * * * * * * * * * * * : * * * * *
```

Figure 7. Sequence alignment of NCX1 among different species. The residue numbering corresponds to the canine NCX1 AD splice variant. The boxed region represents the construct studied in the present work.

Using the Dali server,[65] two-helix bundles with similar geometry as THB are found in the PDB as integral elements of large proteins where they are stabilized by interacting with other secondary structures (Table S2). By contrast, autonomous THB-like domains are notably rare.[66-68] Synthetic two-helix bundles have been created for protein folding studies[69-71] and significant efforts are being devoted to the design of stable miniproteins.[72,73] The THB domain reported here, a new naturally occurring minimal protein domain that is 39 amino acids in length, may serve as a model for protein folding studies and as a template for the design of small proteins with tunable size and stability in the rapidly advancing field of protein engineering and synthetic biology.

ASSOCIATED CONTENT

Supporting Information

The following file is available free of charge.

Supplementary figures (PDF)

Accession Codes

Protein Data Bank entry 6BV7. Biological Magnetic Resonance Bank entry 30379.

AUTHOR INFORMATION

Corresponding Author

* Department of Chemistry and Biochemistry, The Ohio State University, 151 W Woodruff Ave, Columbus, Ohio, 43210, USA. Email: bruschweiler.1@osu.edu. Phone: 614-688-2083.

ORCID

Rafael Brüschweiler: 0000-0003-3649-4543

Author Contributions

J.Y., C.Y., M.X., L.Y. and L.B.-L. conducted experiments. J.Y., C.Y. and R.B. analyzed data. J.Y., C.Y., L.B.-L. and R.B. designed experiments. J.Y., L.B.-L. and R.B. wrote the manuscript.

Funding Sources

This study was supported by the NSF (award MCB-1715505).

Notes

The authors declare no competing financial interest.

ACKNOWLEDGMENT

We thank Drs. Da-Wei Li and Alexandar Hansen for helpful discussions. All computer simulations were done at the Ohio Supercomputer Center.

ABBREVIATIONS

NCX – Na^{+}/Ca^{2+} Exchanger, NMR – nuclear magnetic resonance spectroscopy, THB – two-helix bundle domain, CBD – Ca^{2+} binding domain, HSQC – heteronuclear single quantum coherence spectroscopy, SSP – secondary structure propensity, hetNOE – heteronuclear Overhauser effect

REFERENCES

1. Philipson, K. D., and Nicoll, D. A. (2000) Sodium-calcium exchange: a molecular perspective, *Annu. Rev. Physiol. 62*, 111-133.

2. Baker, P. F., Blaustein, M. P., Hodgkin, A. L., and Steinhardt, R. A. (1969) The influence of calcium on sodium efflux in squid axons, *J. Physiol. 200*, 431-458.

3. Nicoll, D. A., Longoni, S., and Philipson, K. D. (1990) Molecular cloning and functional expression of the cardiac sarcolemmal Na^{+}-Ca^{2+} exchanger, *Science 250*, 562-565.

4. Dyck, C., Omelchenko, A., Elias, C. L., Quednau, B. D., Philipson, K. D., Hnatowich, M., and Hryshko, L. V. (1999) Ionic regulatory properties of brain and kidney splice variants of the NCX1 Na^{+}-Ca^{2+} exchanger, *J. Gen. Physiol. 114*, 701-711.

5. Kang, T. M., and Hilgemann, D. W. (2004) Multiple transport modes of the cardiac $Na^{+/}Ca^{2+}$ exchanger, *Nature 427*, 544-548.

6. Lytton, J. (2007) Na^{+}/Ca^{2+} exchangers: three mammalian gene families control Ca^{2+} transport, *Biochem. J. 406*, 365-382.

7. Khananshvili, D. (2013) The SLC8 gene family of sodium-calcium exchangers (NCX) - Structure, function, and regulation in health and disease, *Mol. Aspects Med. 34*, 220-235.

8. Quednau, B. D., Nicoll, D. A., and Philipson, K. D. (1997) Tissue specificity and alternative splicing of the Na^{+}/Ca^{2+} exchanger isoforms NCX1, NCX2, and NCX3 in rat, *Am. J. Physiol. Cell Physiol. 272*, C1250-C1261.

9. Nicoll, D. A., Ottolia, M., Lu, L., Lu, Y., and Philipson, K. D. (1999) A new topological model of the cardiac sarcolemmal Na^{+}-Ca^{2+} exchanger, *J. Biol. Chem. 274*, 910-917.

10. Matsuoka, S., Nicoll, D. A., Reilly, R. F., Hilgemann, D. W., and Philipson, K. D. (1993) Initial localization of regulatory regions of the cardiac sarcolemmal Na^{+}-Ca^{2+} exchanger, *Proc. Natl. Acad. Sci. U. S. A. 90*, 3870-3874.

11. Liao, J., Li, H., Zeng, W., Sauer, D. B., Belmares, R., and Jiang, Y. (2012) Structural insight into the ion-exchange mechanism of the sodium/calcium exchanger, *Science 335*, 686-690.

12. Abramson, J., Paz, A., and Philipson, K. D. (2012) It's All in the Symmetry, *Science 335*, 669-670.

13. Ren, X., and Philipson, K. D. (2013) The topology of the cardiac Na^{+}/Ca^{2+} exchanger, NCX1, *J. Mol. Cell. Cardiol. 57*, 68-71.

14. Liao, J., Marinelli, F., Lee, C., Huang, Y., Faraldo-Gómez, J. D., and Jiang, Y. (2016) Mechanism of extracellular ion exchange and binding-site occlusion in a sodium/calcium exchanger, *Nat. Struct. Mol. Biol. 23*, 590-599.

15. Giladi, M., van Dijk, L., Refaeli, B., Almagor, L., Hiller, R., Man, P., Forest, E., and Khananshvili, D. (2017) Dynamic distinctions in the Na^{+}/Ca^{2+} exchanger adopting the inward- and outward-facing conformational states, *J. Biol. Chem. 292*, 12311-12323.

16. Nicoll, D. A., Sawaya, M. R., Kwon, S., Cascio, D., Philipson, K. D., and Abramson, J. (2006) The crystal structure of the primary Ca^{2+} sensor of the Na^{+}/Ca^{2+} exchanger reveals a novel Ca^{2+} binding motif, *J. Biol. Chem. 281*, 21577-21581.

17. Besserer, G. M., Ottolia, M., Nicoll, D. A., Chaptal, V., Cascio, D., Philipson, K. D., and Abramson, J. (2007) The second Ca^{2+}-binding domain of the Na^{+}-Ca^{2+} exchanger is essential for regulation: Crystal structures and mutational analysis, *Proc. Natl. Acad. Sci. U. S. A. 104*, 18467-18472.

18. Giladi, M., Sasson, Y., Fang, X., Hiller, R., Buki, T., Wang, Y. X., Hirsch, J. A., and Khananshvili, D. (2012) A common Ca^{2+}-driven interdomain module governs eukaryotic NCX regulation, *PloS one 7*, e39985.

19. Salinas, R. K., Bruschweiler-Li, L., Johnson, E., and Brüschweiler, R. (2011) Ca^{2+} binding alters the interdomain flexibility between the two cytoplasmic calcium-binding domains in the Na^+/Ca^{2+} exchanger, *J. Biol. Chem. 286*, 32123-32131.

20. Giladi, M., Lee, S. Y., Hiller, R., Chung, K. Y., and Khananshvili, D. (2015) Structure-dynamic determinants governing a mode of regulatory response and propagation of allosteric signal in splice variants of Na^+/Ca^{2+} exchange (NCX) proteins, *Biochem. J. 465*, 489-501.

21. Lee, S. Y., Giladi, M., Bohbot, H., Hiller, R., Chung, K. Y., and Khananshvili, D. (2016) Structure-dynamic basis of splicing-dependent regulation in tissue-specific variants of the sodium-calcium exchanger, *FASEB J. 30*, 1356-1366.

22. Giladi, M., Lee, S. Y., Ariely, Y., Teldan, Y., Granit, R., Strulovich, R., Haitin, Y., Chung, K. Y., and Khananshvili, D. (2017) Structure-based dynamic arrays in regulatory domains of sodium-calcium exchanger (NCX) isoforms, *Sci. Rep. 7*, 993.

23. Hilge, M., Aelen, J., Foarce, A., Perrakis, A., and Vuister, G. W. (2009) Ca^{2+} regulation in the Na^+/Ca^{2+} exchanger features a dual electrostatic switch mechanism, *Proc. Natl. Acad. Sci. U. S. A. 106*, 14333-14338.

24. Hilge, M. (2012) Ca^{2+} regulation of ion transport in the Na^+/Ca^{2+} exchanger, *J. Biol. Chem. 287*, 31641-31649.

25. Abiko, L. A., Vitale, P. M., Favaro, D. C., Hauk, P., Li, D. W., Yuan, J., Bruschweiler-Li, L., Salinas, R. K., and Brüschweiler, R. (2016) Model for the allosteric regulation of the Na^{+}/Ca^{2+} exchanger NCX, *Proteins: Struct., Funct., Bioinf. 84*, 580-590.

26. Plain, F., Congreve, S. D., Yee, R. S. Z., Kennedy, J., Howie, J., Kuo, C. W., Fraser, N. J., and Fuller, W. (2017) An amphipathic α-helix directs palmitoylation of the large intracellular loop of the sodium/calcium exchanger, *J. Biol. Chem. 292*, 10745-10752.

27. Khananshvili, D. (2017) How a helix imposes palmitoylation of a membrane protein: What one can learn from NCX, *J. Biol. Chem. 292*, 10753-10754.

28. Li, Z., Nicoll, D. A., Collins, A., Hilgemann, D. W., Filoteo, A. G., Penniston, J. T., Weiss, J. N., Tomich, J. M., and Philipson, K. D. (1991) Identification of a peptide inhibitor of the cardiac sarcolemmal Na^{+}-Ca^{2+} exchanger, *J. Biol. Chem. 266*, 1014-1020.

29. He, Z., Petesch, N., Voges, K. P., Röben, W., and Philipson, K. D. (1997) Identification of important amino Acid residues of the Na^{+}-Ca^{2+} exchanger inhibitory peptide, XIP, *J. Membr. Biol. 156*, 149-156.

30. Hilge, M., Aelen, J., and Vuister, G. W. (2006) Ca^{2+} regulation in the Na^{+}/Ca^{2+} exchanger involves two markedly different Ca^{2+} sensors, *Mol. Cell 22*, 15-25.

31. Showalter, S. A., Bruschweiler-Li, L., Johnson, E., Zhang, F., and Brüschweiler, R. (2008) Quantitative lid dynamics of MDM2 reveals differential ligand binding modes of the p53-binding cleft, *J. Am. Chem. Soc. 130*, 6472-6478.

32. Qin, H., Hu, J., Hua, Y., Challa, S. V., Cross, T. A., and Gao, F. P. (2008) Construction of a series of vectors for high throughput cloning and expression screening of membrane proteins from *Mycobacterium tuberculosis*, *BMC Biotechnol. 8*, 51.

33. Schanda, P., Van Melckebeke, H., and Brutscher, B. (2006) Speeding up three-dimensional protein NMR experiments to a few minutes, *J. Am. Chem. Soc. 128*, 9042-9043.

34. Lescop, E., Schanda, P., and Brutscher, B. (2007) A set of BEST triple-resonance experiments for time-optimized protein resonance assignment, *J. Magn. Reson. 187*, 163-169.

35. Chary, K. V. R., Otting, G., and Wüthrich, K. (1991) Measurement of small heteronuclear ^{1}H-^{15}N coupling constants in ^{15}N-labeled proteins by 3D $H_N NH_{AB}$-COSY, *J. Magn. Reson. 93*, 218-224.

36. Barsukov, I. L., and Lian, L. Y. (1993) Structure determination from NMR data I. Analysis of NMR data, in *NMR of macromolecules: A practical approach* (Roberts, G. C. K., Ed.) 1st ed., pp 315-357, Oxford University Press, Oxford.

37. Senn, H., Werner, B., Messerle, B. A., Weber, C., Traber, R., , and Wüthrich, K. (1989) Stereospecific assignment of the methyl ^{1}H NMR lines of valine and leucine in polypeptides by nonrandom ^{13}C labelling, *FEBS Lett. 249*, 113-118.

38. Diercks, T., Coles, M., and Kessler, H. (1999) An efficient strategy for assignment of cross-peaks in 3D heteronuclear NOESY experiments, *J. Biomol. NMR 15*, 177-180.

39. Brutscher, B., Brüschweiler, R., and Ernst., R. R. (1997) Backbone dynamics and structural characterization of the partially folded A state of ubiquitin by ^{1}H, ^{13}C, and ^{15}N nuclear magnetic resonance spectroscopy, *Biochemistry 36*, 13043-13053.

40. Palmer, A. G., Kroenke, C. D., and Loria, J. P. (2001) Nuclear Magnetic Resonance Methods for Quantifying Microsecond-to-Millisecond Motions in Biological Macromolecules, *Methods Enzymol. 339*, 204-238.

41. Delaglio, F., Grzesiek, S., Vuister, G. W., Zhu, G., Pfeifer, J., and Bax, A. (1995) NMRPipe: A multidimensional spectral processing system based on UNIX pipes, *J. Biomol. NMR 6*, 277-293.

42. Goddard, T. D., and Kneller, D. G. (2008) SPARKY 3, University of California, San Francisco.

43. Johnson, B. A., and Blevins, R. A. (1994) NMR View: A computer program for the visualization and analysis of NMR data, *J. Biomol. NMR 4*, 603-614.

44. Shen, Y., Delaglio, F., Cornilescu, G., and Bax, A. (2009) TALOS+: a hybrid method for predicting protein backbone torsion angles from NMR chemical shifts, *J. Biomol. NMR 44*, 213-223.

45. Brunger, A. T. (2007) Version 1.2 of the Crystallography and NMR system, *Nat. Protoc. 2*, 2728-2733.

46. Bhattacharya, A., Tejero, R., and Montelione, G. T. (2007) Evaluating protein structures determined by structural genomics consortia, *Proteins: Struct., Funct., Bioinf. 66*, 778-795.

47. Kuszewski, J., and Clore, G. M. (2000) Sources of and solutions to problems in the refinement of protein NMR structures against torsion angle potentials of mean force, *J. Magn. Reson. 146*, 249-254.

48. Koradi, R., Billeter, M., and Wüthrich, K. (1996) MOLMOL: a program for display and analysis of macromolecular structures, *J. Mol. Graph 14*, 51-55.

49. Baker, N. A., Sept, D., Joseph, S., Holst, M. J., and McCammon, J. A. (2001) Electrostatics of nanosystems: Application to microtubules and the ribosome, *Proc. Natl. Acad. Sci. U. S. A. 98*, 10037-10041.

50. Dolinsky, T. J., Nielsen, J. E., McCammon, J. A., and Baker, N. A. (2004) PDB2PQR: an automated pipeline for the setup of Poisson-Boltzmann electrostatics calculations, *Nucleic Acids Res. 32*, W665-667.

51. Abraham, M. J., Murtola, T., Schulz, R., Páll, S., Smith, J. C., Hess, B., and Lindahl, E. (2015) GROMACS: High performance molecular simulations through multi-level parallelism from laptops to supercomputers, *SoftwareX 1*, 19-25.

52. Li, D.-W., and Brüschweiler, R. (2010) NMR-based protein potentials, *Angew. Chem. Int. Ed. 49*, 6778-6780.

53. Piana, S., Donchev, A. G., Robustelli, P., and Shaw, D. E. (2015) Water dispersion interactions strongly influence simulated structural properties of disordered protein states, *J. Phys. Chem. B 119*, 5113-5123.

54. Buchan, D. W., Minneci, F., Nugent, T. C., Bryson, K., and Jones, D. T. (2013) Scalable web services for the PSIPRED Protein Analysis Workbench, *Nucleic Acids Res. 41*, W349-357.

55. Roy, A., Kucukural, A., and Zhang, Y. (2010) I-TASSER: a unified platform for automated protein structure and function prediction, *Nat. Protoc. 5*, 725-738.

56. Marsh, J. A., Singh, V. K., Jia, Z., and Forman-Kay, J. D. (2006) Sensitivity of secondary structure propensities to sequence differences between α- and γ-synuclein: Implications for fibrillation, *Protein Sci. 15*, 2795-2804.

57. Montelione, G. T., Nilges, M., Bax, A., Güntert, P., Herrmann, T., Richardson, J. S., Schwieters, C. D., Vranken, W. F., Vuister, G. W., Wishart, D. S., Berman, H. M., Kleywegt, G. J., and Markley, J. L. (2013) Recommendations of the wwPDB NMR Validation Task Force, *Structure 21*, 1563-1570.

58. Aurora, R., and Rose, G. D. (1998) Helix capping, *Protein Sci. 7*, 21-38.

59. Andreotti, A. H. (2003) Native state proline isomerization: an intrinsic molecular switch, *Biochemistry 42*, 9515-9524.

60. de la Torre, J. G., Huertas, M. L., and Carrasco, B. (2000) HYDRONMR: Prediction of NMR relaxation of globular proteins from atomic-level structures and hydrodynamic calculations, *J. Magn. Reson. 147*, 138-146.

61. Debiec, K. T., Cerutti, D. S., Baker, L. R., Gronenborn, A. M., Case, D. A., and Chong, L. T. (2016) Further along the Road Less Traveled: AMBER ff15ipq, an Original Protein Force Field Built on a Self-Consistent Physical Model, *J. Chem. Theory Comput. 12*, 3926-3947.

62. John, S. A., Ribalet, B., Weiss, J. N., Philipson, K. D., and Ottolia, M. (2011) Ca^{2+}-dependent structural rearrangements within Na^{+}-Ca^{2+} exchanger dimers, *Proc. Natl. Acad. Sci. U. S. A. 108*, 1699-1704.

63. Zhou, H.-X. (2004) Polymer models of protein stability, folding, and interactions, *Biochemistry 43*, 2141-2154.

64. Hryshko, L. V., Matsuoka, S., Nicoll, D. A., Weiss, J. N., Schwarz, E. M., Benzer, S., and Philipson, K. D. (1996) Anomalous regulation of the *Drosophila* Na^{+}-Ca^{2+} exchanger by Ca^{2+}, *J. Gen. Physiol. 108*, 67-74.

65. Holm, L., and Rosenstrom, P. (2010) Dali server: conservation mapping in 3D, *Nucleic Acids Res. 38*, W545-549.

66. Sun, Y., Parker, M. H., Weigele, P., Casjens, S., Prevelige, P. E., Jr., and Krishna, N. R. (2000) Structure of the coat protein-binding domain of the scaffolding protein from a double-stranded DNA virus, *J. Mol. Biol. 297*, 1195-1202.

67. Dodson, C. A., and Arbely, E. (2015) Protein folding of the SAP domain, a naturally occurring two-helix bundle, *FEBS Lett. 589*, 1740-1747.

68. Ng, Y. M., Yang, Y., Sze, K. H., Zhang, X., Zheng, Y. T., and Shaw, P. C. (2011) Structural characterization and anti-HIV-1 activities of arginine/glutamate-rich polypeptide Luffin P1 from the seeds of sponge gourd (Luffa cylindrica), *J. Struct. Biol. 174*, 164-172.

69. Lai, J. K., Kubelka, G. S., and Kubelka, J. (2015) Sequence, structure, and cooperativity in folding of elementary protein structural motifs, *Proc. Natl. Acad. Sci. U. S. A. 112*, 9890-9895.

70. Baker, E. G., Williams, C., Hudson, K. L., Bartlett, G. J., Heal, J. W., Porter Goff, K. L., Sessions, R. B., Crump, M. P., and Woolfson, D. N. (2017) Engineering protein stability with atomic precision in a monomeric miniprotein, *Nat. Chem. Biol. 13*, 764-770.

71. Fezoui, Y., Connolly, P. J., and Osterhout, J. J. (1997) Solution structure of αtα, a helical hairpin peptide of de novo design, *Protein Sci. 6*, 1869-1877.

72. DeGrado, W. F., Summa, C. M., Pavone, V., Nastri, F., and Lombardi, A. (1999) De novo design and structural characterization of proteins and metalloproteins, *Annu. Rev. Biochem. 68*, 779-819.

73. Rocklin, G. J., Chidyausiku, T. M., Goreshnik, I., Ford, A., Houliston, S., Lemak, A., Carter, L., Ravichandran, R., Mulligan, V. K., Chevalier, A., Arrowsmith, C. H., and Baker, D. (2017) Global analysis of protein folding using massively parallel design, synthesis, and testing, *Science 357*, 168-175.

For Table of Contents Use Only

The Intracellular Loop of the Na^{+}/Ca^{2+} Exchanger Contains an "Awareness Ribbon" Shaped Two-helix Bundle Domain

Jiaqi Yuan[1], Chunhua Yuan[2], Mouzhe Xie[1], Lei Yu[1], Lei Bruschweiler-Li[2],

and Rafael Brüschweiler[,1,2,3]*